Periodic Evolution of Multiscale Precipitation Systems Developed within a Baiu Frontal Cloud Cluster

Yasutaka WAKAZUKI, Kazuhisa TSUBOKI, and Takao TAKEDA

Hydrospheric Atmospheric Research Center, Nagoya University, Nagoya, Japan

(Manuscript received 29 November 2002, in final form 15 February 2006)

Abstract

A meso-α-scale cloud cluster (CC) was observed in the Baiu frontal zone, located southwest of Kyushu, Japan, on July 7, 1996. It was characterized by a lifespan of approximately 20 hours, stationary motion, and heavy precipitation of over 200 mm in a period of 12 hours. This paper contains a report of the characteristic features of internal multiscale precipitation systems observed within the CC, and their periodic evolutions as newly found facts.

The CC consisted of a convective rainfall region, characterized by a meso-β_L-scale (100–200 km) line-shaped convective system (convective line, Mβ_LCL), and a weak stratiform rainfall region on the lee side of the Mβ_LCL. The Mβ_LCL consisted of several band-shaped meso-β_S-scale (20–100 km) convective systems (Mβ_SCSs), and each Mβ_SCS consisted of meso-γ-scale cumulonimbus clouds. The environmental atmosphere was characterized by a warm and moist inflow in the shallow layer (below 500 m in height) associated with a cyclonic circulation of slow moving and shallow depression. Additionally, the CC was located within a large temperature gradient zone in the lower atmosphere (below 4000 m in height) along the Baiu front. These were favorable environments for the generation and maintenance of the Mβ_LCL. The Mβ_LCLs were periodically generated with an interval of 5–6 hours in almost the same region, and they showed a common evolution of structure and processes.

The behavior of cold pools formed by the Mβ_LCLs on the northern side of the Mβ_LCL played a key role in the periodic evolution. The developed cold pool intensified the Mβ_SCSs in the Mβ_LCL and modified one of the Mβ_SCSs into an arc-shaped Mβ_SCS, that had similar characteristics to those of squall lines. Simultaneously, the arc-shaped Mβ_SCS became the sole Mβ_SCS that constituted Mβ_LCL. Finally, the Mβ_LCL decayed with the expansion of the cold pool. Another Mβ_LCL was generated when the favorable environment was restored after the cold pool dissipated, and the evolution process of the Mβ_LCL was repeated.

1. Introduction

The Baiu frontal zone in East Asia is characterized by wide and quasi-stationary precipitation, and cloud zones extending zonally from East China to the Japan Islands. A large amount of rainfall is brought over the Baiu frontal zone in Japan in June and July. In the Baiu frontal zone, several types of heavy rainfall events are observed. One of them is the meso-α-scale cloud cluster (CC). Here, the scales are based on the scale definition of Orlanski (1975). Meso-α-scale CCs bring an extremely large amount of rainfall (200–500 mm/day), in a narrow area and sometimes cause serious disasters. They are often observed around the Kyushu District (western Japan), especially during the late Baiu season (early July). Many researchers (e.g., Ninomiya et al. 1988a, b; Ishihara et al. 1995; Kato 1998; Seko 2000) have studied the characteristic features and dynamic structures of CCs by observations and numer-

Corresponding author and present affiliation: Yasutaka Wakazuki, Advanced Earth Science and Technology Organization, Meteorological Research Institute (MRI), Tsukuba 305-0052, Japan.
E-mail: ywakazki@mri-jma.go.jp

ical experiments. However, the generation, development, and maintenance mechanisms of CCs have not been thoroughly explained, because of the lack of spatial and temporal observational data for meso-α-scale precipitation phenomena.

One of the important problems for the study of meso-α-scale CCs is their complicated internal multiscale structures. The complexity is caused by the interaction among large-scale dynamics, mesoscale convective organizations, and cloud micro-physics. The multiscale structure of CCs was found in the Global Atmospheric Research Project's Atlantic Tropical Experiment (GATE). The small-scale precipitation systems were embedded inside the CCs (e.g., Leary and Houze 1979). Moreover, Mesoscale Convective Complexes (MCCs) (Maddox 1980), which are often observed in North America, have been reported to include convective precipitation systems.

Meso-α-scale CCs in the Baiu frontal zone have been found to have internal multiscale structures on the case analyses of observations. Iwasaki and Takeda (1989) identified the multiscale structure within a quasi-stationary meso-α-scale CC observed around the Kyushu District. The CC consisted of meso-β-scale low-T_{BB} cloud groups. The generation of new meso-β-scale convective cloud groups, with a period of about 1 hour on the up-shear side, resulted in the stagnation and maintenance of the CC. A meso-β-scale convective cloud group consisted of several meso-γ-scale cumulonimbus clouds. Ninomiya et al. (1988a) also pointed out the multiscale structure of a meso-α-scale CC. The CC moved slowly because internal meso-β-scale convective systems were generated on the up-shear side of the CC for a period of about 5 hours. Thus, the characteristic features of the multiscale structures of CCs in the Baiu frontal zones were determined to be periodic occurrences, or alignments, of convective systems within the CCs. In addition, the periodicities play a role in the behavior of CCs. However, the dynamic mechanisms of their periodicities have not been sufficiently explained. On the other hand, in some studies, there have been reports of the periodicities of heavy rainfall (Matsumoto and Akiyama 1969; Matsumoto and Tsuneoka 1969; Akiyama 1978; Ninomiya 1983). These periodic variations were explained in association with gravity waves. However, the relationship between the multiscale structure and periodicities has not been clarified. Periodicities of different scales, with different dynamic processes, are expected in a multiscale structure.

An intense observation project called TREX (Torrential Rain Experiment; e.g., Kato et al. 1998; Seko 2000) targeted mesoscale precipitation systems in the Baiu frontal zone, and was performed in southern Kyushu in June and July, 1996. In the project, radiosondes with high spatial resolution were launched, and X-band Doppler radars were installed in the vicinity of the radiosonde launching points. In this paper, a case analysis of observational data of a meso-α-scale CC, observed on July 7, 1996 is reported. In this case, a multiscale structure of convective precipitation systems was observed within the CC. In addition, the precipitation systems showed a significant periodic evolution. These characteristic features are newly identified in this study, although the multiscale structure had some similarities to those in cases of Iwasaki and Takeda (1989) and Ninomiya et al. (1988a). In Sections 2, 3, and 4 of this paper, data descriptions, the atmospheric environment around the CC, and the characteristics of the CC are respectively introduced. We focus on the periodic evolution of precipitation systems, and the multiscale structure of the CC in Section 5, by introducing a suitable sub-scale definition. We also clarify the relationship between the periodic evolution and the multiscale structure of the CC. Finally, we discuss the mechanisms of the periodic evolution, in association with the multiscale structure and the Baiu frontal environment in Section 6. The summary is presented in Section 7.

2. Data

The CC was generated at around 21 JST (i.e., JST = UTC + 9 hours) July 6, 1996 over the East China Sea to the southwest of the Kyushu District, and decayed at around 17 JST July 7. Figure 1 is a typical T_{BB} distribution of the CC. Figure 1 also contains a map of the observation area in the present study. Infrared T_{BB} data of the Geostationary Meteorological Satellite (GMS)-5 were used to observe the cloud distribution of the CC. The C-band quantitative meteorological radar, located on Tanegashima

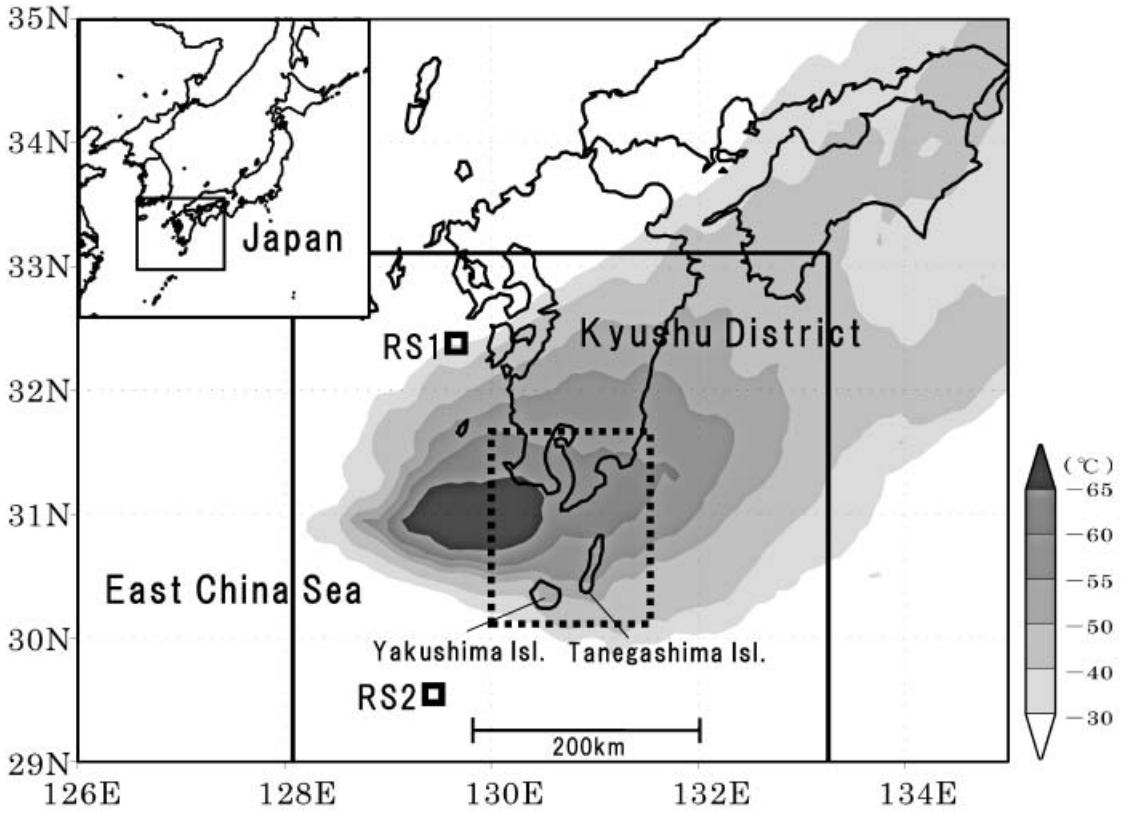

Fig. 1. Study domain and T_{BB} distribution of the CC averaged for the period from 04 JST to 13 JST July 7, 1996. The box region is the data domain of the C-band quantitative radar. The open squares are the radiosonde launching points of RS1 (on the vessel) and RS2 (at Tairajima). The dotted box region is a domain of Fig. 2.

Island, was used to analyze the distribution of wide-range precipitation, and detect the meso-β-scale and meso-γ-scale convective systems. The precipitation amount was estimated by using the Radar-Automated Meteorological Data Acquisition System (AMeDAS) composite precipitation data, i.e., radar-integrated rainfall data, calibrated by surface raingauge data.

Upper sounding radiosonde data, at six points around the CC, and the grid point value of the Regional Spectrum Model (RSM), were used to derive a thermodynamic environment. In particular, the profiles at RS1 and RS2 were used as representatives of the northern and southern sides of the CC, respectively (Fig. 1). Other radiosonde launching points, shown in Fig. 2, were located near the CC. These radiosonde data were not assimilated to the objective analysis data (RANAL), which was used for the initial data of the RSM. The radiosondes were launched every 3 hours at RS1, while others were launched at 21 JST July 6 and 09 JST July 7. The data of the surface meteorological observation around the CC (Fig. 2), including AMeDAS data (SS1-5 and SS7-10) and special observation data (SS6), were used to estimate the thermodynamic variations at the surface. The surface observation at SS6 had been stopped as a result of a thunderbolt accident at 0920 JST.

Two X-band Doppler radars of the Hydrospheric Atmospheric Research Center (HyARC), Nagoya University, and the Meteorological Research Institute (MRI), Japan Meteorological Agency (JMA), were installed in Tanegashima and Yakushima Islands, respectively. The time intervals of the volume scans were 7 and 14 minutes, respectively. The observation ranges of the radars were 64 km. The data of the Doppler radars were used to study

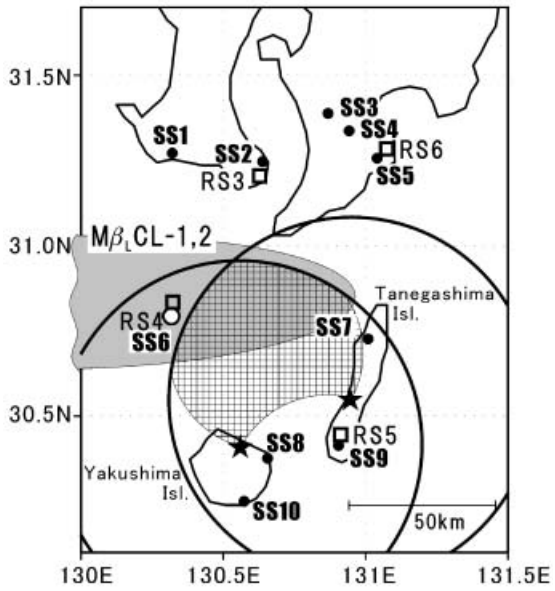

Fig. 2. Close-up map of the region of intensive field observation over southern Kyushu. The open squares are radiosonde launching points of RS3, RS4, RS5, and RS6 (at Yamakawa, Ioujima, Minamitane, and Uchinoura, respectively). The closed circles (SS1-5 and SS7-10) are Automated Meteorological Data Acquisition System (AMeDAS) points of JMA around both meso-β_L-scale convective lines-1 and -2 (gray oval) defined in Section 5.2. The open circle (SS6) is the special observation point at Ioujima. The two star marks are the Doppler radar sites, and the two large circles with a radius of 64 km are their ranges. The hatched region is the dual Doppler analysis area.

the structures of meso-β-scale, and meso-γ-scale convective systems in the CC. Dual Doppler analyses were performed to derive the three-dimensional wind velocities around the convective systems.

3. Environmental atmosphere

The Baiu front is characterized by large meridional gradients of temperature and humidity in the lower atmosphere, and a moist air transport along the Low Level Jet (LLJ) around the levels of 900–700 hPa. Figures 3a, 3c, and 3d show the environmental fields around the CC at 03 JST July 7, 1996, derived from the RSM output, with an initial time at 21 JST July 6. The CC developed into a meso-α-scale at that time, which was 6 hours after the generation of the CC. The Baiu frontal zone was located at the 31–33°N latitudinal range around the Kyushu District. The CC was generated around the southernmost end of the Baiu frontal zone. At 1000 hPa (Fig. 3a), a large meridional gradient of equivalent potential temperature (θe) was present along the Baiu frontal zone. In particular, a high-θe south-southwesterly inflow toward the Baiu front, and the CC was significantly observed on the southern side of the CC at 03 and 09 JST (Figs. 3a and 3b). At 900 hPa and 700 hPa (Figs. 3c and 3d), the southwesterly or west-southwesterly wind was dominant around the CC. The LLJ was especially significant in the Baiu frontal zone. A moist air transport was observed mainly on the northern side of the LLJ axis, which is known as the moist tongue.

Figure 3 also shows that a meso-α-scale depression was present over the East China Sea. The depression was located on the northwestern side of the CC. It accompanied an upper-level cut-off vortex and a trough (not shown). The depression was generated at around 21 JST July 6 over the East China Sea near the Korean Peninsula. The movement of the depression, which is shown by time labels in Fig. 3c, was about 6 ms^{-1} toward the southeast. The depression was shallow and confined to below 700 hPa. The south-southwesterly on the southern side of the CC at 1000 hPa, was associated not only with a quasi-stationary anti-cyclonic circulation of the subtropic high over the Pacific Ocean, but also with a cyclonic circulation of the depression.

Figure 4 shows the sounding profiles at RS1-6 at 09 JST July 7. At RS1 (Fig. 4a), which was located on the northern side of the CC, the level of free convection (LFC) was not present, because the temperature was low below about 500 m in height. At RS2, which was located on the southern side of the CC, a strong conditionally unstable layer was present below 1500 m in height, because of an extremely warm layer below 1000 m in height. The high-θe air was also present below about 1000 m in height. However, the LFC was estimated to be high (about 2000 m in height). Therefore, it was difficult for deep convections to be generated on

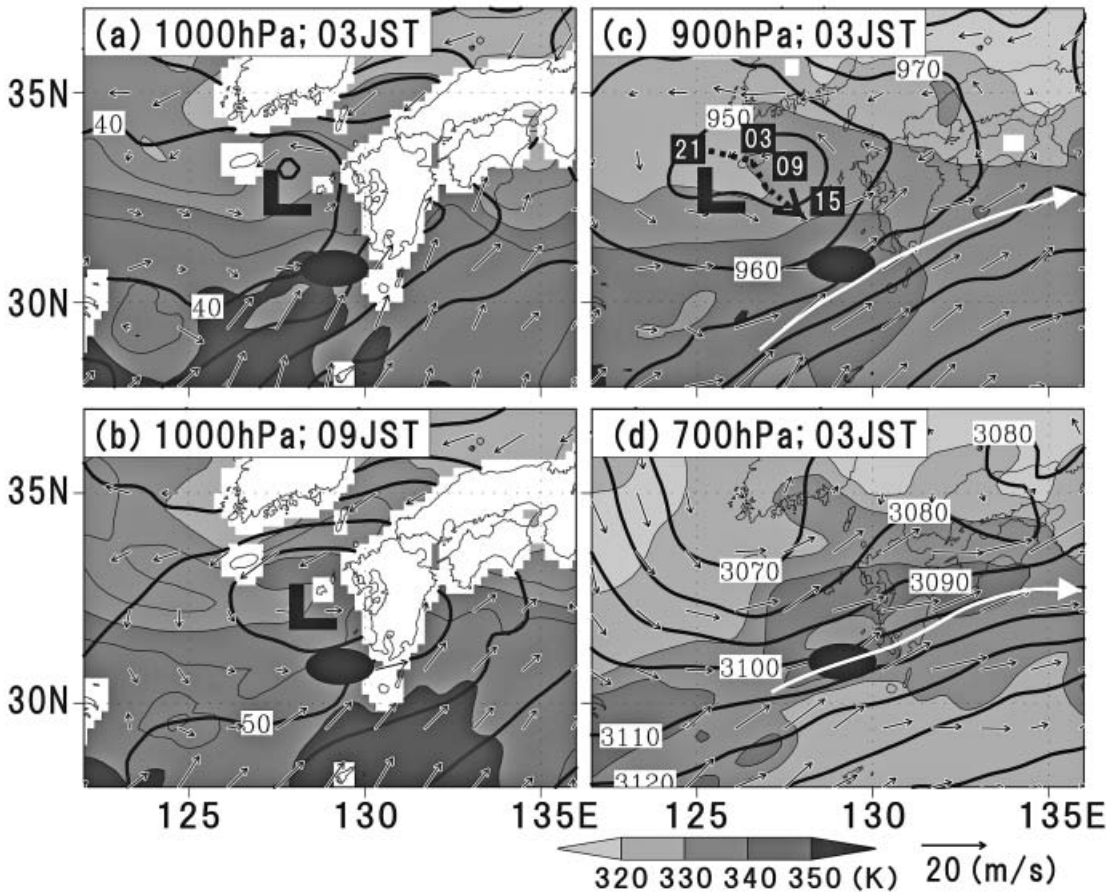

Fig. 3. Large-scale atmospheric fields at (a, c, and d) 03 JST and (b) 09 JST July 7, 1996 derived from the Regional Spectrum Model (RSM) output: geopotential height every 10 m (contoured), equivalent potential temperature (shaded), and horizontal velocities (arrows) at the (a, b) 1000, (c) 900, and (d) 700 hPa levels. The closed ovals are the position of the CC. "L" is the depression observed around the CC. The dotted black arrow in (c) is the track of the depression at 900 hPa. Numbers near the arrow refer to the passage time of the depression (JST). The white arrows in (c) and (d) are the axes of the large wind speed zones. The initial time of the RSM is 21 JST July 6, 1996.

both the northern and southern side of the CC under that condition. On the other hand, convectively neutral conditions were present around the CC at RS3, RS4, and RS6, because of convections within the CC (the θe profiles at these points are not shown).

A favorable condition for the CC to be generated is the significant southerly high-θe air inflow in the shallow layer (below 500 m in height) associated with the depression. Figure 5 shows the convective available potential energy (CAPE), and convective inhibition (CIN), for the air parcel at a height of 100 m at 03 and 09 JST July 7 derived from the RSM output. A large CAPE was present around the CC and on the southern side of the CC. The large CAPE around the CC was produced mainly by the high-θe air in the shallow layer. On the other hand, Fig. 4c shows that the southerly component of the wind had a local maximum around 500 m in height at RS2, while that above 1 km in height was small. The large southerly component of the inflow is also present in Figs. 3a and 3b. The inflow efficiently and successively carried the high-θe air in the shallow layer toward the CC. Consequently, for example, the θe below 500 m in height at RS5 located near the CC, was almost the same

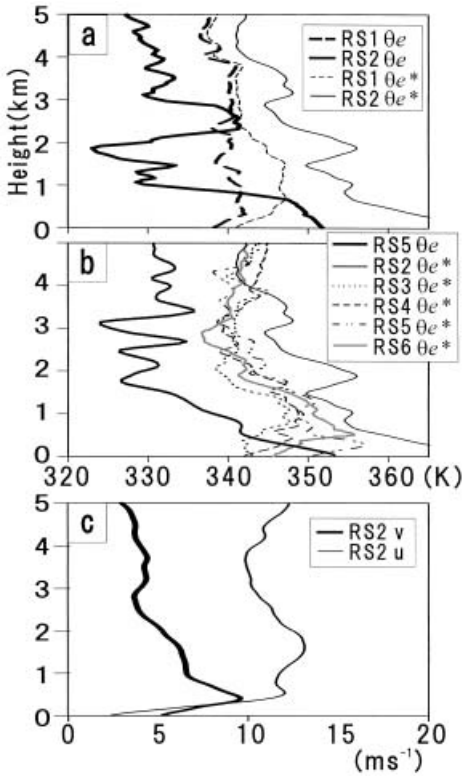

Fig. 4. Sounding profiles at 09 JST July 7, 1996, observed at RS1-6: (a) θe and saturated equivalent potential temperature (θe^*) at RS1 and RS2, (b) θe at RS5 and θe^* at RS2-6, and (c) zonal and meridional components of the wind velocity (u, v) at RS2.

as that of about 350 K at RS2 (Fig. 4b). Thus, the large CAPE around the CC was maintained mainly by the high-θe advection in the shallow layer, and decayed with the eastward propagation of the high-θe air shown in Figs. 3a and 3b.

Another favorable condition for the CC to be generated is a small CIN around the CC (Fig. 5). In order to produce a low LFC, associated with a small CIN for the high-θe air advected in the shallow layer, a lower saturated equivalent potential temperature (θe^*) than that at RS2 in the lower atmosphere is required around the CC. Figure 4b shows that the θe^* at RS3–6 (located around the CC) was much lower than that at RS2 below 4 km in height. Consequently, for example, the LFC at RS5 is estimated to be about 500 m in height, while that at RS2 was 2000 m in height. Thus, quasi-stationary large meridional gradients of θe^*, and temperature in the lower atmosphere (below 4000 m in height) is important for the high-θe air in the shallow layer to produce a small CIN. Figure 6 shows the temperature averaged within the levels from 950 to 850 hPa at 03 and 09 JST derived from the RSM output. The large meridional gradient of the temperature extends in an almost zonal direction around the CC at both 03 and 09 JST, and was mostly maintained around the CC until the CC decayed. Here, the temperature gradient is a large-scale characteristic feature in the Baiu frontal zone.

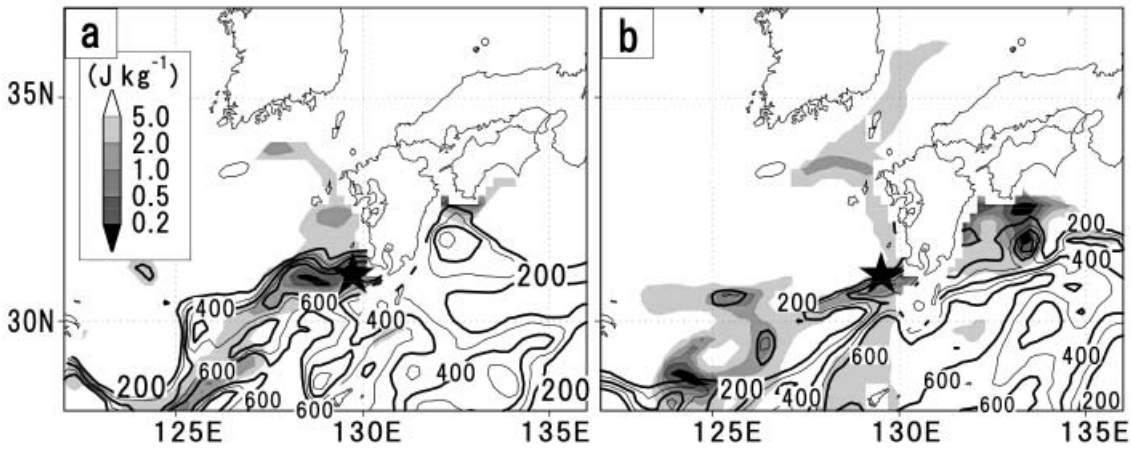

Fig. 5. CAPE (contoured every 200) and CIN (shaded) of an air parcel at a height of 100 m at (a) 03 and (b) 09 JST July 7 derived from the RSM. The units are J kg^{-1}. The star marks are the position of the CC.

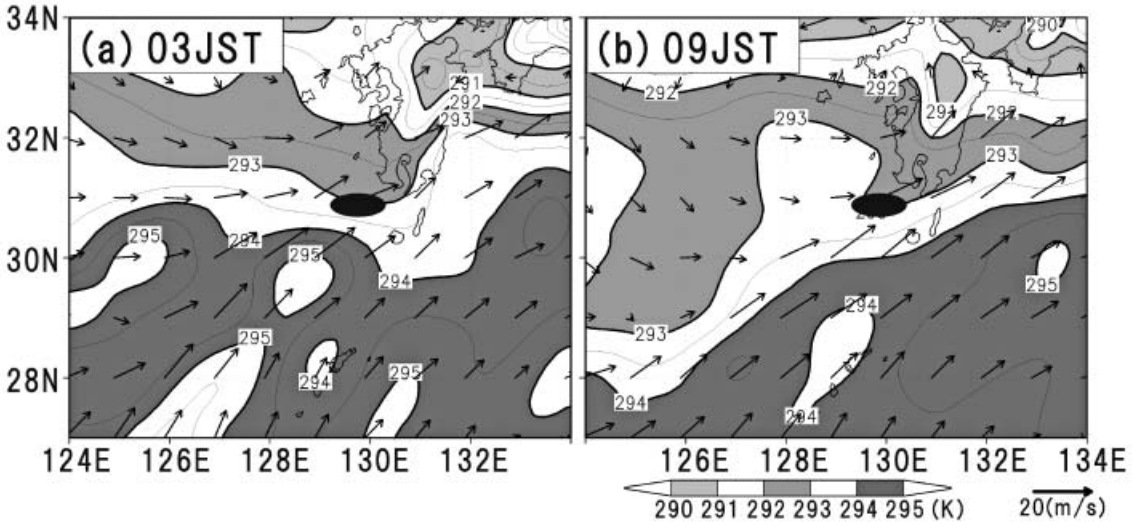

Fig. 6. The temperature (contoured every 1 K and shaded) and horizontal velocities (arrows) averaged within the levels from 950 to 850 hPa at (a) 03 and (b) 09 JST derived from the RSM. The closed ovals are the position of the CC.

4. Characteristics of a cloud cluster

Figure 7 shows the time series of the GMS Infrared T_{BB} and radar echo reflectivity distributions of the CC. The CC had a life span of approximately 20 hours until its decaying at around 17 JST July 7. The CC was almost stationary during its evolution. The CC brought a large amount of rainfall in a narrow area. The total rainfall amount in the region covered by the CC, and maximum rainfall for 12 hours in a 5-km mesh, are estimated by the Radar-AMeDAS composite rainfall data, to be about 6.5×10^9 m^3 and 200 mm, respectively. The large amount of rainfall was attributed to the long life span and the characteristic of stationariness of the CC. The CC was also accompanied by deep convective clouds, and their minimum T_{BB} reached -78°C, which was over 15 km in height.

In this study, the evolution of the CC is divided into three stages. The period from 21 JST July 6 to 02 JST July 7, is defined as the developing stage. In this stage, the CC developed dramatically, and low T_{BB} cloud regions, which correspond to anvil clouds generated by deep convections, extended rapidly. Several heavy rainfall features were conspicuously present and were accompanied by meso-β-scale low T_{BB} convective clouds. Meanwhile, regions with weak rainfall were not widespread in the CC. The period from 02 JST to 13 JST July 7, is defined as the mature stage. In this stage, the CC developed into a meso-α-scale cloud system (c.f. 03 JST), and retained the scale throughout the stage. The CC was almost stationary during this stage, even though the mean environmental wind was not weak. The T_{BB} was lower in the western part (on the windward side) of the CC than that in the eastern part. In the western part of the CC, concentrated intense rainfall regions were observed, and heavy rainfall features were embedded within the rainfall regions. The heavy rainfall almost corresponded to cloud regions lower than -70°C of T_{BB}, which were intermittently present. In the eastern part, the weak rainfall region spread widely below anvil clouds of the CC on the lee side of the intense rainfall region. These situations were maintained for about 11 hours. Finally, the period after 13 JST July 7, is defined as the decaying stage. In this stage, no heavy rainfall features were present in the CC. This study focuses on the maintenance processes and evolution of precipitation systems in the mature stage of the CC in the following sections.

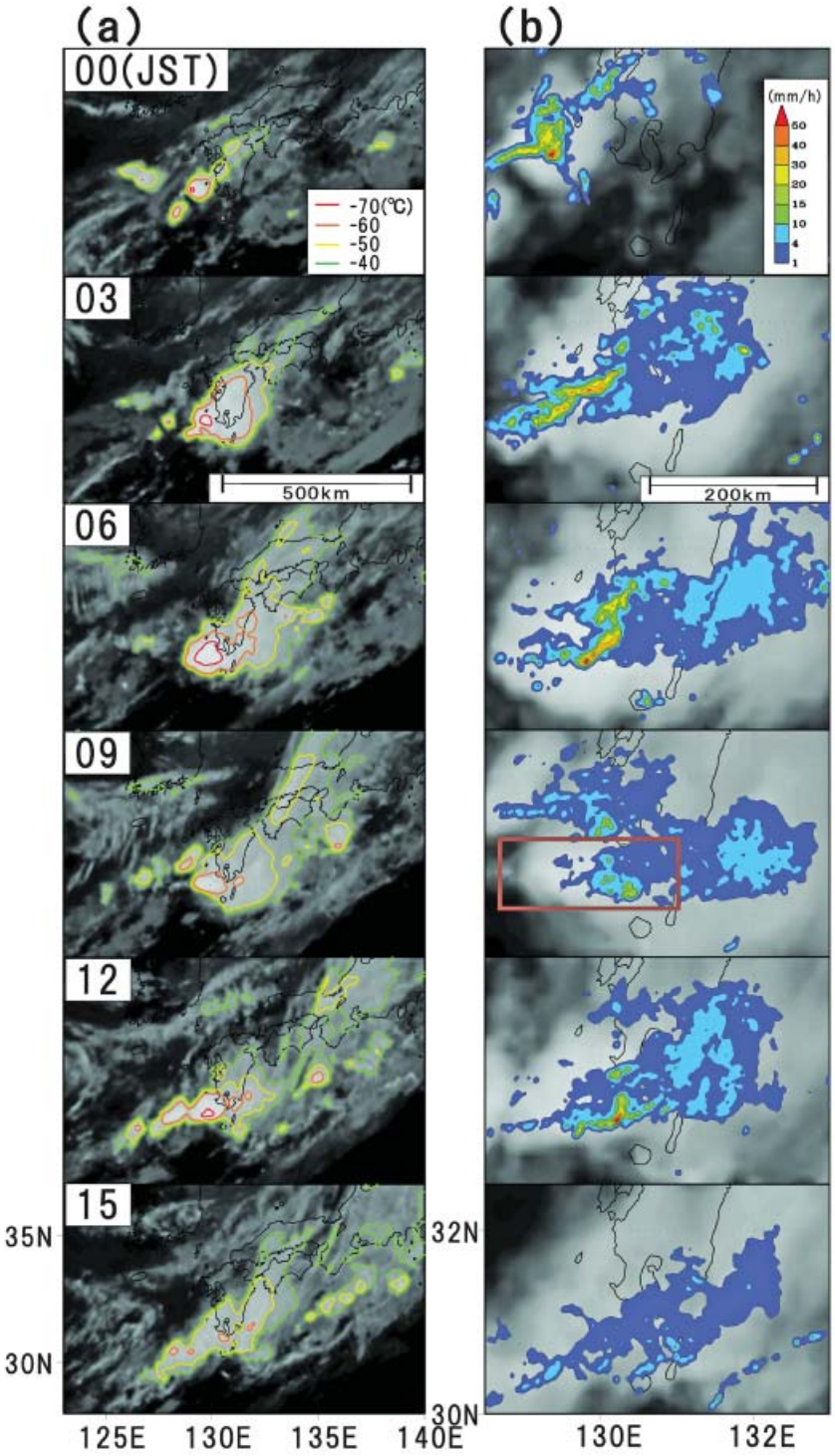

Fig. 7. (a) Time variations of the T_{BB} distributions of the CC every 3 hours from 00 to 15 JST July 7. The T_{BB} is contoured every 10°C. The white regions show low T_{BB} clouds, and the brighter white indicates the lower clouds. (b) Same as in (a) but magnified, and the radar echo reflectivity (rainfall rate) distributions (color) are superimposed. The brown box region at 09 JST in (b) is a domain in Fig. 8.

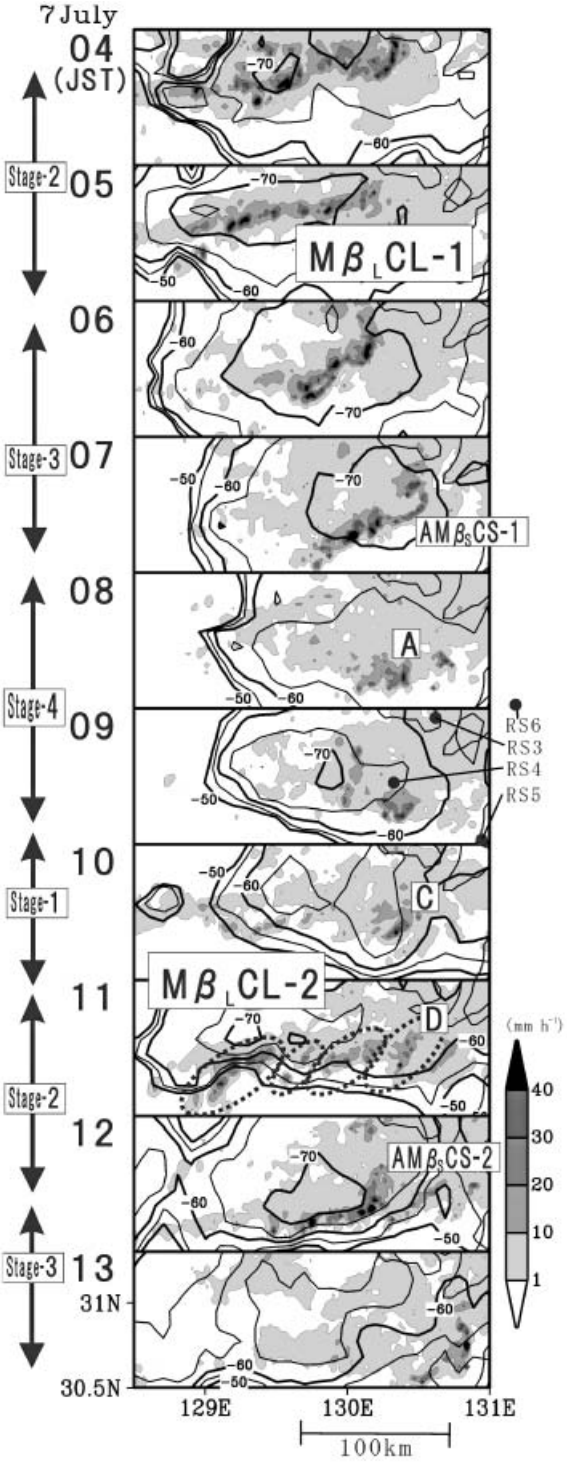

5. Multiscale structure of the precipitation systems within a cloud cluster in the mature stage

5.1 Subdivision of the meso-β-scale

In this section, we focus on the multiscale structure of precipitation systems within the CC in the mature stage. For the description of the multiscale structure in the present study, the meso-β-scale is divided into two sub-scales. Horizontal scales of 20–100 km and 100–200 km are defined as the meso-β_S-scale and meso-β_L-scale, respectively. An almost identical definition has been given by Seko (2000). These scale classifications are not generally used, but are suitable to describe the multiscale structure in the present case.

5.2 Multiscale structure

Figure 8 shows the time variations of the radar echo reflectivity and T_{BB} distributions in the mature stage every hour, focusing on the intense rainfall regions located in the western part of the CC. Convective radar echoes aligned almost zonally, and had line shapes at 05 JST and 11 JST. The lengths of the line-shaped convective systems were about 200 km. We define them as the meso-β_L-scale convective lines (Mβ_LCLs). The whole shape of the Mβ_LCL at 05 JST (Mβ_LCL-1) became less clear by 07 JST, and a weak rainfall region spread widely on the northern side of the Mβ_LCL-1. After the decaying of Mβ_LCL-1 at 08 JST, only the weak rainfall region spread widely with scattered convective echoes. The scale of the weak rainfall region was the meso-β_L-scale. Another Mβ_LCL (Mβ_LCL-2) was generated in almost the same region, in which Mβ_LCL-1 was located

Fig. 8. Time variation of the radar echo reflectivity (rainfall rate) and the T_{BB} distributions (contoured) in the mature stage every hour. The closed circles at 09 JST indicate the locations of RS3, RS4, RS5, and RS6. The dotted circles at 11 JST are the Mβ_SCSs in Mβ_LCL-2. The letters A, C, and D are the labels of the Mβ_SCSs identified in Fig. 17. The AMβ_SCSs-1 and -2 defined in Fig. 14 are also labeled. The domain is shown in Fig. 7b. The stages of the Mβ_LCL defined in Section 5.3 are also shown.

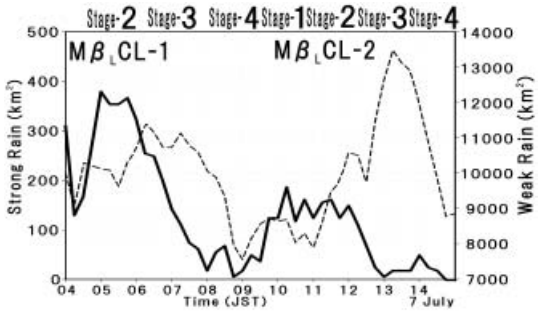

Fig. 9. Time variations of the area of strong radar-echo reflectivity (solid line; the rainfall rate is stronger than 30 mm h^{-1}) and that of weak radar-echo reflectivity (dashed line; the rainfall rate is weaker than 10 mm h^{-1}) in the mature stage. The region of the calculation is 128.5–131 E and 30.5–31.5°N, which is the same as the domain of Fig. 8. The stages of the Mβ_LCL defined in Section 5.3 are also shown.

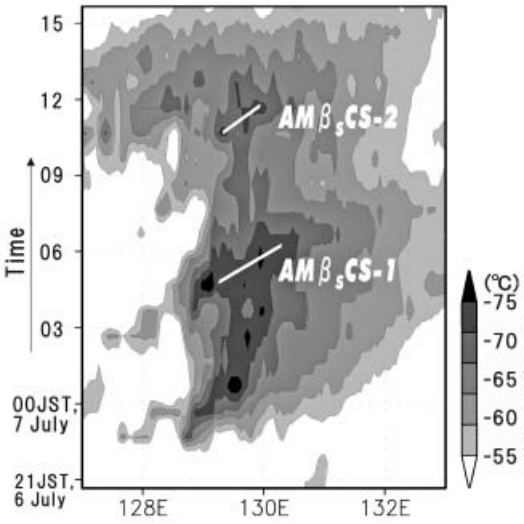

Fig. 10. Time-longitude cross section of the minimum T_{BB} within the latitudinal range of 25–35°N. The two white lines indicate the movements of AMβ_SCSs-1 and -2 defined in Section 5.3.

previously after the weak rainfall weakened (at 10 JST). The line shape of Mβ_LCL-2 became clear by 11 JST. The evolution of the structures for Mβ_LCL-2 after its generation at around 10 JST, was almost the same as that of the structure for Mβ_LCL-1.

Figure 9 shows the time variations of the echo areas of strong ($R \geq 30$ mm h^{-1}) and weak ($R \leq 10$ mm h^{-1}) radar reflectivity. The strong rainfall echo area was large from 0430 to 0700 JST and from 1000 to 1200 JST. These periods correspond to those in which the Mβ_LCLs were conspicuously present. On the other hand, the weak rainfall echo area was large in the periods from 0600 to 0800 JST and from 1130 to 1430 JST. The periods followed those in which the Mβ_LCLs were present. The time intervals for the generation of the Mβ_LCLs were 5–6 hours. The life spans of the Mβ_LCLs were about 2.5 hours. The time interval from the decaying of an Mβ_LCL to the generation of the next Mβ_LCL was about 3 hours. Two or more Mβ_LCLs were not simultaneously observed.

Figure 10 shows the time-longitude cross section of the minimum T_{BB} within a latitudinal range of 25–35°N. No other deep convections were observed within the latitudinal range. When the Mβ_LCLs were present (at around 04 and 11 JST) and at around 00 JST (in the developing stage), cloud regions lower than −70°C of T_{BB} were significantly observed. They were located in almost the same longitudinal positions. The intermittent generation of the Mβ_LCLs in almost the same regions at around 04 and 10 JST (Fig. 8), resulted in the stationariness of the CC.

We focus on the internal structure of the Mβ_LCL. The Mβ_LCL consisted of smaller-scale convective radar echo groups. As an example, they are shown by four ovals at 11 JST in Fig. 8. The scales of these echoes were from 50 to 100 km. They are defined as the meso-β_S-scale convective systems (Mβ_SCSs). They moved to the east within the Mβ_LCLs. Many of them were band-shaped, with orientations from southwest to northeast, or west-southwest to east-northeast. Figure 11 shows the time variation of the radar echo distributions of Mβ_LCL-2 every 7.5 minutes, focusing on the generation process of the Mβ_LCL-2. The four Mβ_SCSs in Fig. 8 are shown by ovals in the bottom panel of Fig. 11. They are defined as band-shaped Mβ_SCSs. Their life spans and periodic intervals were 1–3 hours and about 1 hour, respectively.

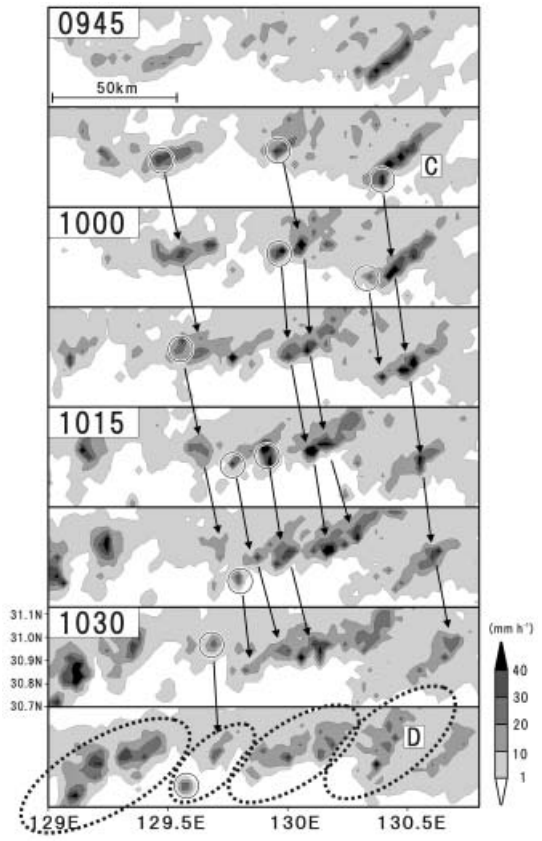

Fig. 11. Time variation of the radar echo reflectivity (rainfall rate; mm hr^{-1}) distribution every 7.5 minutes. The circles indicate the newly generated meso-γ-scale convective cellular echoes. The arrows indicate the movements of cellular echoes. The dotted ovals in the bottom panel are the Mβ_SCSs within Mβ_LCL-2. Letters C and D are the labels of the Mβ_SCSs identified in Fig. 17.

They consisted of several meso-γ-scale cellular echoes associated with cumulonimbus clouds. The circles in Fig. 11 are newly generated meso-γ-scale convective cellular echoes. The new convective cells were generated at the southwest edge of the band-shaped Mβ_SCSs. Each band-shaped Mβ_SCS developed, and was maintained by successive generations of meso-γ-scale cumulonimbus clouds. The formation processes of band-shaped Mβ_SCSs are categorized as the back-building-type, defined by Bluestein and Jain (1985).

5.3 *Evolution of the Mβ_LCL*

We will now focus on the evolution and life cycle of the Mβ_LCL. The evolution of the Mβ_LCL is divided into four stages. The first stage (stage 1) is characterized by the generation of the Mβ_LCL. Mβ_LCLs-1 and -2 were generated at around 04 and 10 JST, respectively (Fig. 8). The generation of Mβ_LCL-2 was induced in a short time range of about 40 minutes at around 10 JST (Fig. 8). The Mβ_SCSs within Mβ_LCL-2 aligned along the southwestern edge of the weak stratiform rainfall region, that was present at around 08 and 09 JST.

The second stage (stage 2) is characterized by the development of the Mβ_LCL and the formation of a weak rainfall region on the northern side of the Mβ_LCL. The weak rainfall regions began to spread about 1.5 hours after the generation, and about 1 hour before the decaying of the Mβ_LCLs (at around 11 JST in Fig. 9). In addition to the spread of the weak rainfall region, cold pools were also generated on the northern side of the Mβ_LCLs. Figure 12 shows the time variations of surface temperatures, and the meridional component of the wind at SS1-5 and SS7-10. The points of SS1-5 and SS8-10 were located at about 50 km north and south from the Mβ_LCLs, respectively (Fig. 2). The southerly components of the winds were significant, while irregularity variations were conspicuous (Figs. 12c and 12d). They are consistent with the southwesterly wind environment. On the southern side of the Mβ_LCLs, the temperatures increased with time by 12 JST (Fig. 12b). The increases seemed to be mainly due to the southwesterly environmental warm air advection. On the other hand, decreases in the temperatures were observed at around 06 and 11 JST, at several points on the northern side of the Mβ_LCLs (Fig. 12a). The decreases were more significant at SS3-5, located on the lee side (northeastern side) of the Mβ_LCLs. The low temperatures at these points continued for several hours after the decreases. The decreases were preceded, about 1 hour, by the generation of the Mβ_LCLs, and were accompanied by the spread of the weak rainfall regions shown in Figs. 8 and 9. Thus, the low temperatures seemed to correspond to the cold pools, formed by the Mβ_LCL. The scale of the cold pool is estimated to be the meso-β-scale by the distribution of surface observation points, at

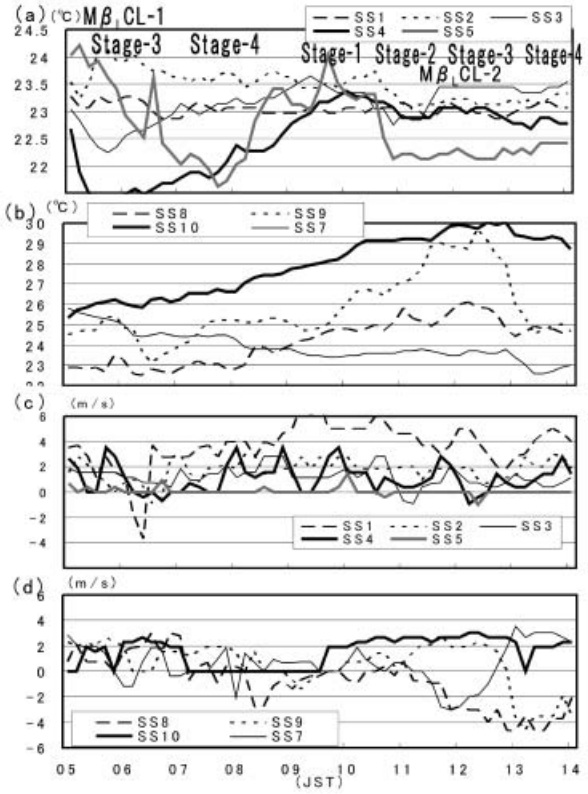

Fig. 12. Time variations of the surface temperature at (a) SS1-5 and (b) SS7-10 and the meridional component of the wind at (c) SS1-5 and (d) SS7-10 observed every 10 minutes. The stages of the Mβ_LCL are also shown.

which the low temperatures were observed (Figs. 2 and 12a). Figure 13 shows the time variations of the sea level pressure at SS1, SS7, and SS8. The sea level pressures were not observed at other AMeDAS points. The sea level pressure on the northern side of the Mβ_LCLs (SS1) had local maximums in stage 2 or 3 in comparison with the average at SS1, SS7, and SS8. These high pressure departures are associated with the generations, and developments of cold pools on the northern side of the Mβ_LCLs.

The third stage (stage 3) is characterized by the decaying of the Mβ_LCL. Figure 14 shows the time variations of radar echo distributions every 15 minutes, focusing on the decaying of the Mβ_LCLs. The band-shaped Mβ_SCSs, aligned along the Mβ_LCLs at 0530 JST and 1030 JST. One of the Mβ_SCSs, located in the western part of Mβ_LCLs-1 and -2, intensified with the eastward movement until 0715 and 1215 JST, respectively. The intensified Mβ_SCSs in Mβ_LCLs-1 and -2, which are traced in Fig. 14, varied into arc-shapes (bow shapes). They are defined as arc-shaped Mβ_SCS (AMβ_SCS). The AMβ_SCSs at around 07 JST in Mβ_LCL-1, and at around 12 JST in Mβ_LCL-2, are named AMβ_SCS-1 and AMβ_SCS-2, respectively. Their developments were accompanied by the disappearances of other Mβ_SCSs on the western side of the AMβ_SCSs (at around 0630 and 1200 JST). Only the AMβ_SCSs remained as unique strong rainfall elements which consti-

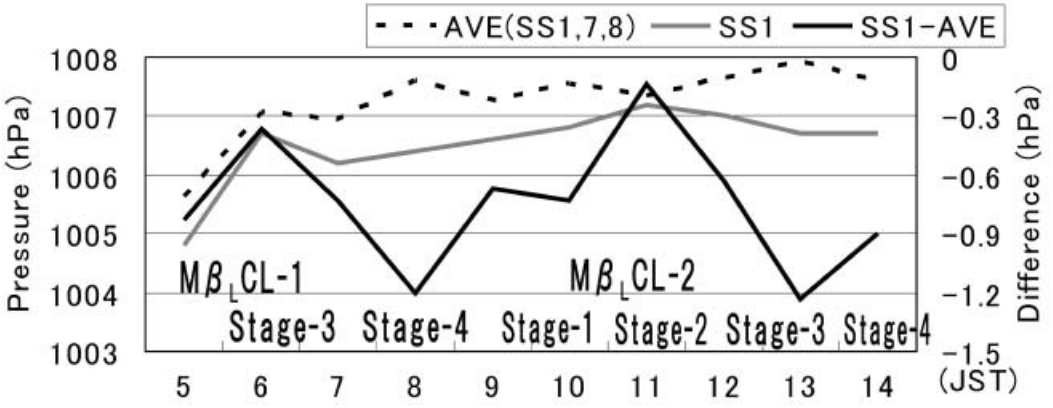

Fig. 13. Time variations of the sea level pressure averaged of SS1, SS7, and SS8 (AVE), that of SS1, and the difference of SS1 from AVE. These are observed every 1 hour. The stages of the Mβ_LCL are also shown.

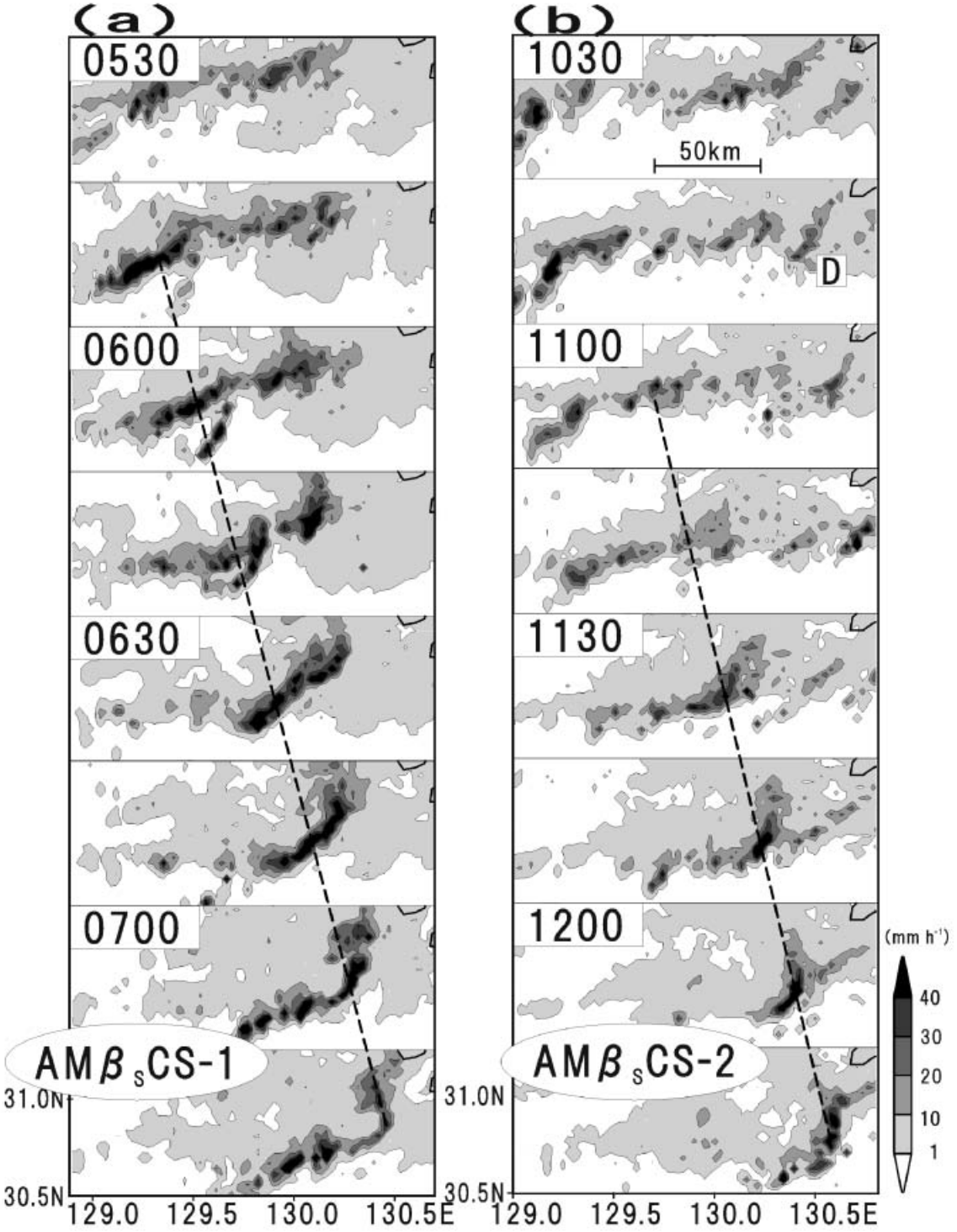

Fig. 14. Time variations of the radar echo reflectivity (rainfall rate) distributions of (a) AMβ_SCS-1 in Mβ_LCL-1 and (b) AMβ_SCS-2 in Mβ_LCL-2 every 15 minutes. AMβ_SCSs-1 and -2 are traced by dashed lines. Letter D is the label of the Mβ_SCS identified in Fig. 17.

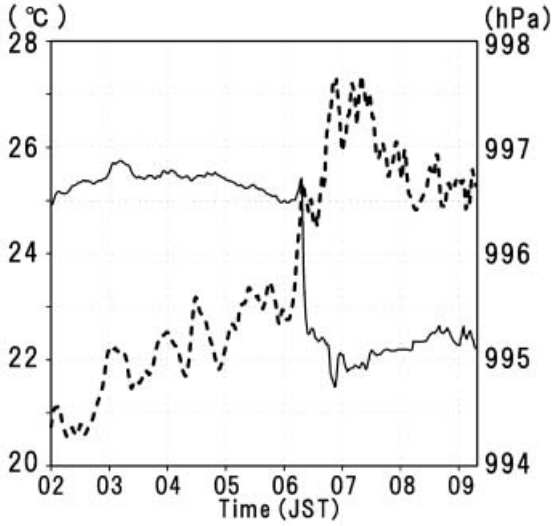

Fig. 15. Time variations of the surface temperature (solid line) and pressure (dotted line) at SS6.

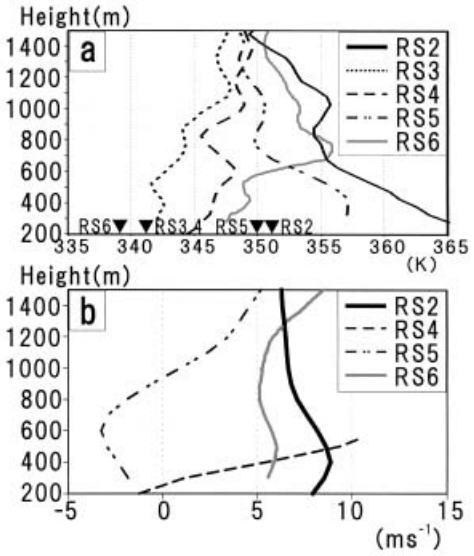

Fig. 16. Radiosonde profiles at RS2-6 below 1500 m in height at 09 JST: (a) θe^* and (b) meridional wind velocities. The triangles in panel (a) represent the θe at 200 m in height at these points. The locations of RS3, RS4, RS5, and RS6 are shown in Figs. 2 and 8.

tuted Mβ_LCLs. At the same time, the weak rainfall region generated on the northern side of the Mβ_LCL, spread further to the west of the AMβ_SCSs. Consequently, the weak rainfall region expanded to the south. Thus, the structures of the Mβ_LCLs which appeared in stage 2 significantly changed in stage 3.

The AMβ_SCSs were accompanied by heavy rainfall and deep convective clouds. Figure 10 shows that the movements of AMβ_SCSs-1 and -2 mostly correspond to those of low T_{BB} cores in the Mβ_LCLs. The AMβ_SCSs moved fast, and their speeds were about 18 m s^{-1} toward the east-southeast direction. The speed was faster than that of other Mβ_SCSs, which was about 12 m s^{-1}. It was also faster than the environmental wind along the LLJ, which was 12–15 m s^{-1}. Figure 15 shows the time variations of surface temperature and surface pressure at SS6. AMβ_SCS-1 passed SS6 at around 0620 JST. When AMβ_SCS-1 passed, a rapid decrease in the temperature of about 2 K, and an increase in the pressure of about 1.5 hPa were observed. Moreover, the low temperature and high pressure after the rapid variations were maintained for at least 3 hours. The SS6 was located in the weak rainfall region after Mβ_LCL-1 decayed. The low temperature and high pressure for 3 hours also suggest the existence of a cold pool behind AMβ_SCS-1 (on the northwestern side).

In the fourth stage (stage 4), only weak rainfall regions spread widely. Figure 16a shows the θe^* profiles and θe at the surface. They are derived from the radiosondes of RS2-6 at 09 JST. The distributions of radiosondes are shown in Figs. 2 and 8. The RS3, RS4, and RS6 were located in the weak rainfall region, and RS2 and RS5 were located on the southern side and around the boundary of the weak rainfall region, respectively. The θe^* profiles at RS2 and RS5 appear to be conditionally unstable, because of the higher temperature in the lower atmosphere. Nevertheless, the LFC was sufficiently high to inhibit convections. On the other hand, the θe^* profiles at RS3, RS4, and RS6 appear to be statically stable because of low temperatures in the lower atmosphere, and the LFC was not present at these points. The difference in the surface temperatures between RS5 and RS4 was about 3 K, which was the largest difference among those between adjacent radiosondes (not shown). The low temperature suggests that the cold pool covered RS3, RS4, and RS6.

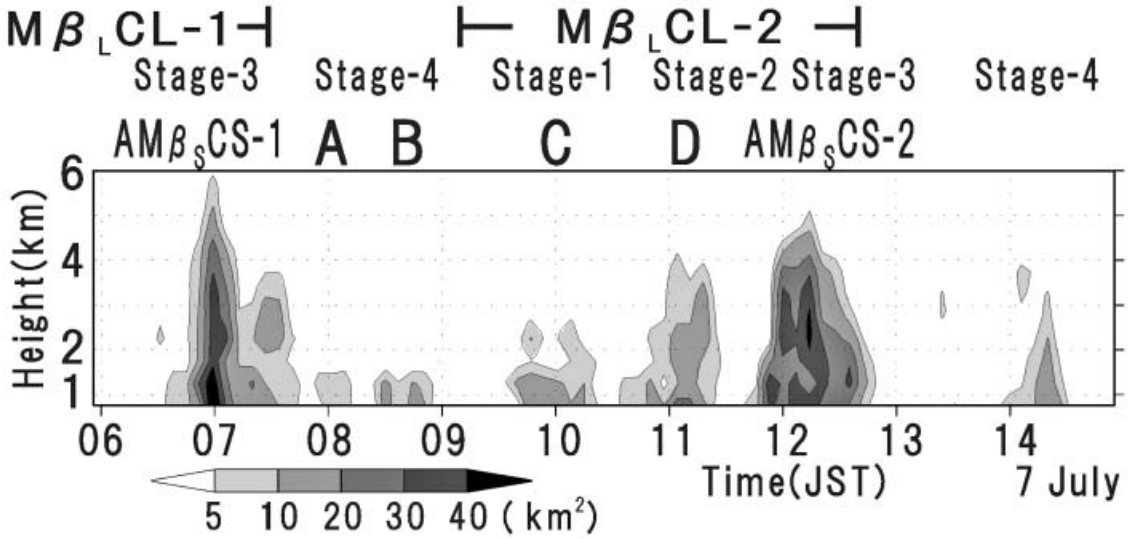

Fig. 17. Time-height cross section of the area of Doppler radar reflectivity larger than 45 dBZ from 06 JST to 15 JST. Letters from A to D and AMβ_SCS-1 and -2 are the labels of the Mβ_SCSs in the Mβ_LCLs. The stages of the Mβ_LCLs defined in Section 5.2 are also shown.

On the other hand, the southerly components of the wind had a maximum of around 500 m in height at RS2 (Fig. 16b). The large southerly is the environmental wind on the southern side of the CC (Figs. 3a and 3b). In contrast, the southerly components of the wind at RS4 and RS5 were small in the lower atmosphere. Moreover, that at RS6 was large in the lower atmosphere once again. The divergence among RS4, RS5, and RS6 was estimated at about 3×10^{-4} s^{-1} below 500 m in height. The large divergence and low temperatures at RS3, RS4, and RS6 suggest that the cold pool generated in stages 2 and 3 was expanding.

Figure 12d shows that the northerly components of the winds were observed at some points on the southern side of the Mβ_LCLs in stages 3 and 4, especially at around 13 JST. There were cases in which the northerly winds were accompanied by decreases in temperature (Fig. 12b). It is suggested that the northerly winds are associated with the horizontal divergences, and the expansions of the cold pool generated on the northern side of the Mβ_LCLs.

5.4 Doppler radar observation

The Mβ_SCSs in the Mβ_LCL were observed by two Doppler radars. The Doppler radars covered Mβ_SCSs in the eastern part of the Mβ_LCL. The structures of the Mβ_SCSs which passed within the radar range and their evolutions were examined.

An index defined as an area of Doppler radar reflectivity larger than 45 dBZ is used. AMβ_SCSs-1 and -2 and four band-shaped Mβ_SCSs labeled from A to D, with variable depths are identified by the time-height cross section of the index (Fig. 17). The Mβ_SCSs are also shown in Figs. 8, 11, and 14. Mβ_SCSs-A and -B are isolated in the weak rainfall region after Mβ_LCL-1 had decayed. They were shallow radar echoes. Mβ_SCSs-C and -D in Mβ_LCL-2 were band-shaped Mβ_SCSs. Mβ_SCSs-C and -D and AMβ_SCS-2 in Mβ_LCL-2 had deep convections, and the heights of the index increased with time from Mβ_SCS-C to AMβ_SCS-2.

The constant-altitude plan-positioning indicators (CAPPIs) at 2 km in height of these Mβ_SCSs are shown in Fig. 18. The structure of AMβ_SCS-1 was not fully observed because some part of the AMβ_SCS-1 was outside of the observation range. Mβ_SCSs-B, -C, and -D had band shapes and developed under the low-level southwesterly winds (Figs. 18b, 18c, and 18d, respectively). The southwesterly wind was largely influenced by the environmental wind in the lower atmosphere on the southern side of the CC, as shown in Fig. 3. The directions of

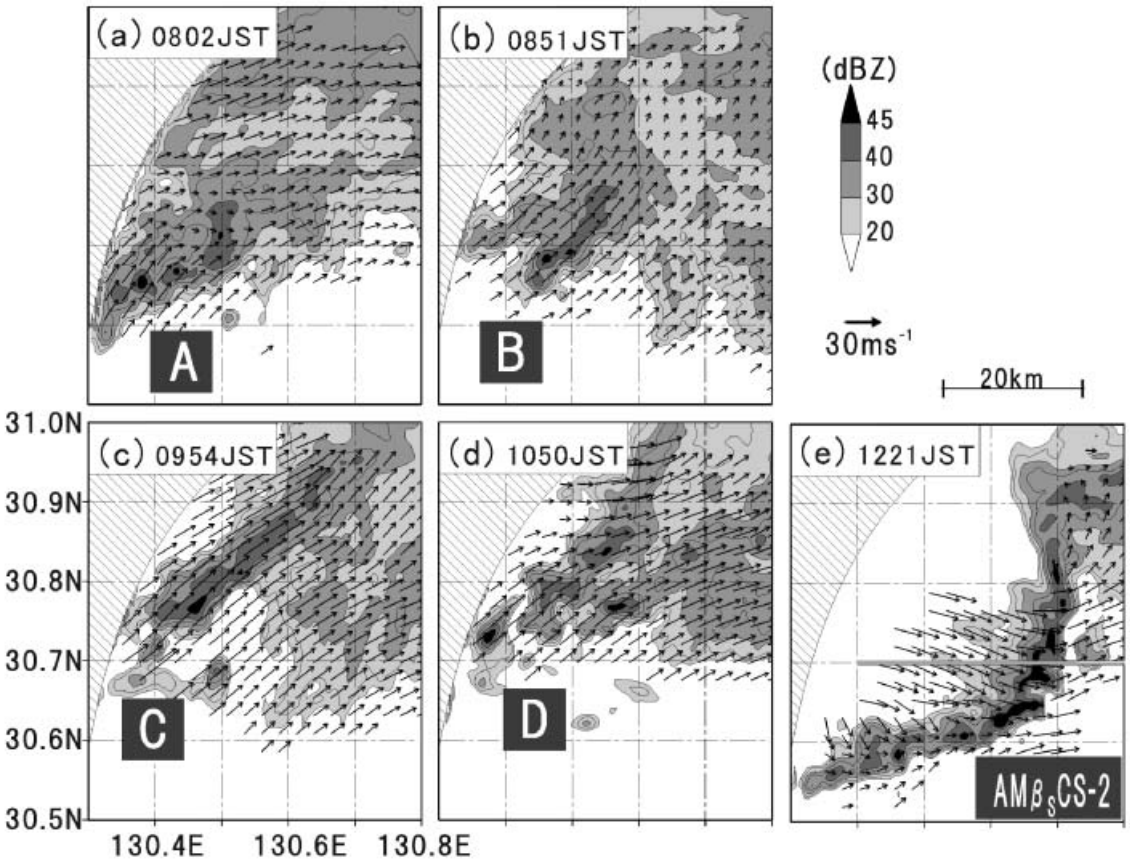

Fig. 18. The CAPPI of the reflectivity (shaded) and horizontal velocity derived from the Doppler radar analysis (arrows) at a height of 2 km in association with the Mβ_SCSs from A to D and AMβ_SCS-2. Hatched regions are outside of the radar range.

the axes of the Mβ_SCSs were almost parallel to the low-level wind. New meso-γ-scale cumulonimbus cellular echoes, which constituted the Mβ_SCSs, were generated to the southwestern edge of the Mβ_SCSs by the back-building-type processes. On the other hand, AMβ_SCS-2 was accompanied by a significant inflow on the rear side (west-northwesterly wind on the western side) and southwesterly wind on the front side of the AMβ_SCS-2 (Fig. 18e). The rear inflow and the southwesterly wind in front of the leading edge made a convergence and a cyclonic wind pattern. The movement velocity of AMβ_SCS-2 was about 18 m s^{-1} toward the east-southeast direction (not shown). Figure 19 shows the vertical cross section along the line in Fig. 18e. The wind arrows in Fig. 19 are the relative wind velocity to the movement of AMβ_SCS-2. A significant rear inflow was observed below 2 km in height. The updraft was tilted toward the rear side, suggesting that AMβ_SCS-2 has characteristics similar to those of asymmetric squall lines. Moreover, AMβ_SCS-1 have several characteristics in common with AMβ_SCS-2: the arc shape structure, fast movement, deep convection, and characteristics of their evolution.

Time variations of the averaged horizontal winds, obtained by dual Doppler radar analyses, are examined in association with the evolution of Mβ_LCL-2 described in Section 5.3 (Fig. 20). When Mβ_LCL-2 was present (when Mβ_SCSs-C, -D, and AMβ_SCS-2 were observed), the southwesterly wind was dominant below 5 km in height (Fig. 20a). It was significant in stages 1 and 2. The southwesterly wind was largely influenced by the environmental wind in the lower atmosphere on the southern side

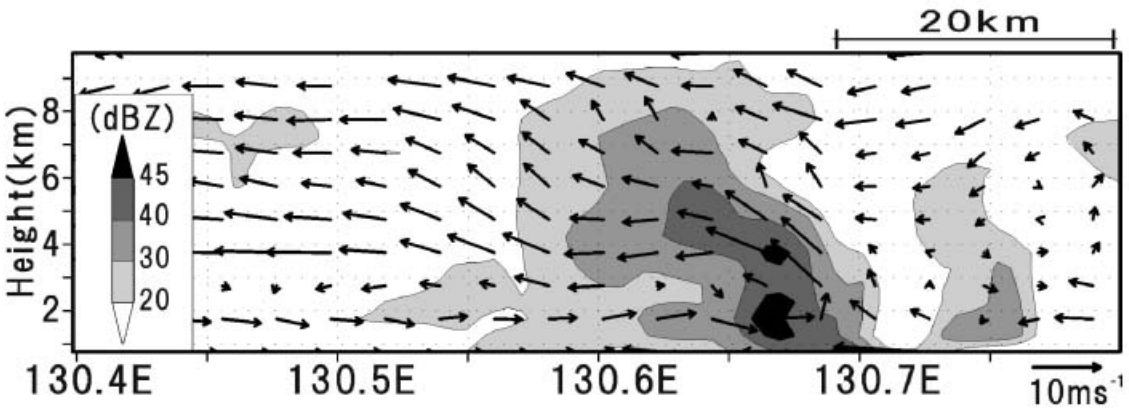

Fig. 19. Vertical cross section of the reflectivity (shaded) and the Doppler velocity (arrows) of AMβ_SCS-2 along the line at 30.7°N in Fig. 18e. The components of the arrows are the zonal velocity relative to the movement of AMβ_SCS-2 and the vertical velocity.

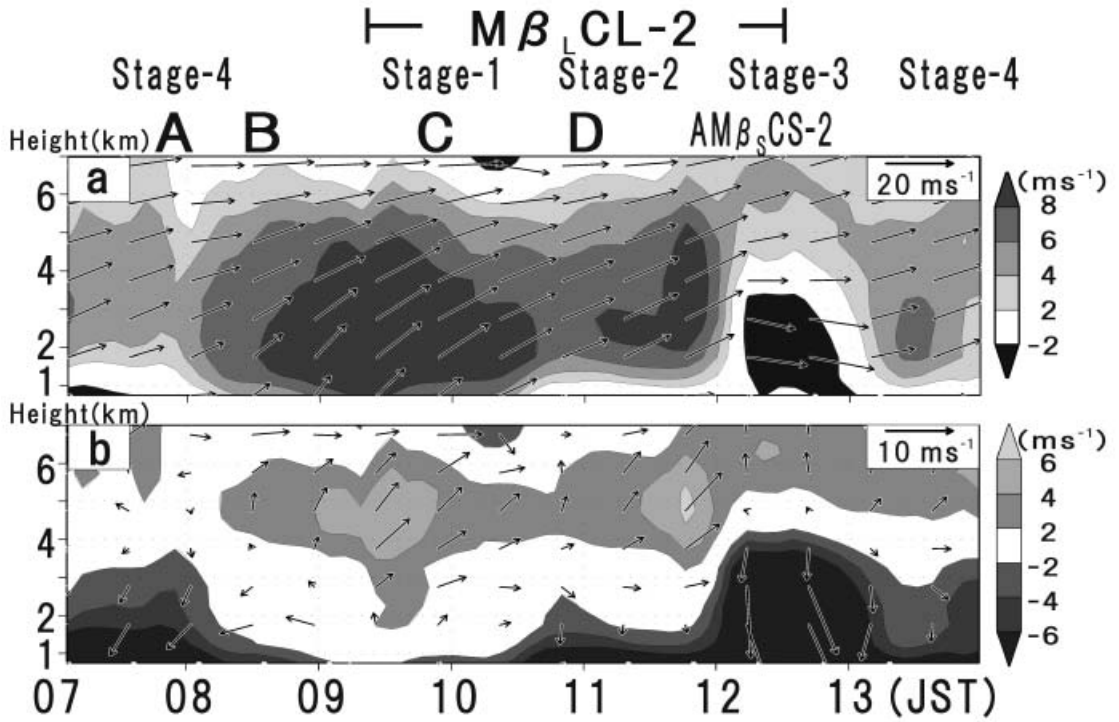

Fig. 20. (a) Time-height cross section of the averaged horizontal wind velocity (arrows) and its meridional component (shaded) estimated by the dual Doppler analysis. The components of the arrows are the zonal and meridional directions. (b) Same as in (a), but the arrows are the velocities relative to the environmental wind derived from the RSM and averaged within 129–131°E and 29.5–30.5°N. Letters from A to D and AMβ_SCS-2 are the same as the letters in Fig. 17. The stages of the Mβ_LCL are also shown.

of the CC. At 1030–1200 JST in stage 2, the meridional wind component was small below 2 km in height. The meridional wind was weak, for example, in the northern part of Mβ_SCS-D (Fig. 18d). In stage 3, at 12–13 JST, the significant northerly wind was observed in the lower atmosphere, which was the rear inflow toward AMβ_SCS-2. In stage 4, the meridional wind component was small below 2 km in height by 09 JST and after 13 JST (Fig. 20a). The weak meridional wind was found, for example, in the northern part of Mβ_SCS-A (Fig. 18a). The weak meridional wind in stage 4 was also observed at RS4 (Fig. 16b). A variation from stage 4 of Mβ_LCL-1 to stage 1 of Mβ_LCL-2 at around 09 JST, was characterized by the dissipation of the weak meridional wind, and the restoration of the southwesterly wind below 2 km in height associated with the environmental southwesterly inflow.

The time variations of the mean velocities were accompanied by the variation of surface temperature and pressure on the northern side of the Mβ_LCLs. When the southwesterly wind below 2 km in height was not significant in stages 2, 3, and 4, the low temperatures were also observed at some points of SSs on the northern side of the Mβ_LCLs (Fig. 12a). These variations show that the environmental warm air inflow in the shallow layer did not sufficiently reach the northern side of the Mβ_LCLs in stages 2, 3, and 4. Moreover, the winds below 2 km in height in stages 2, 3, and 4 had the northerly components of the wind in the relative wind field to the environmental wind derived from the RSM output (Fig. 20b). The relatively northerly winds are considered to be outflows of the cold pools. Moreover, reductions of the high pressure departures on the northern side of the Mβ_LCLs were observed mainly in stage 3 (Fig. 13). They were also consistent with the outflow and expansion of the cold pools.

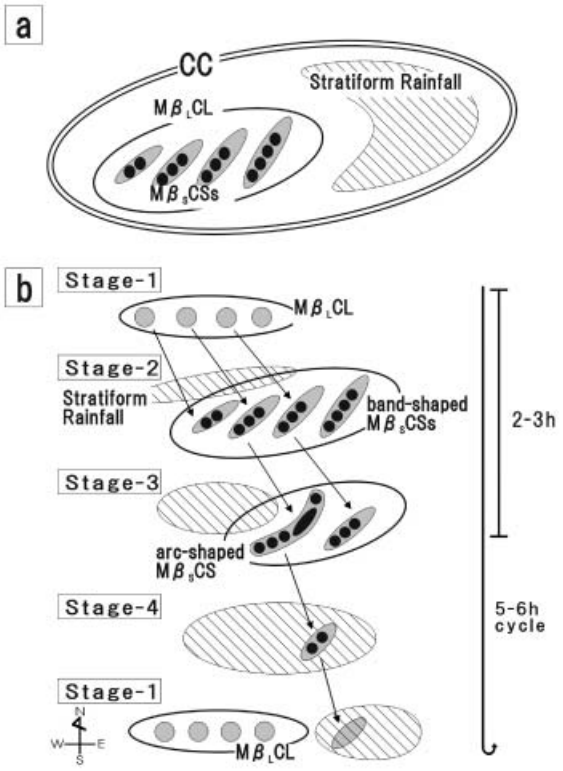

Fig. 21. Schematic features of (a) the multiscale structure of the CC and (b) the periodic evolution of the Mβ_LCLs. Only the convective region (western part) of the CC is focused on in (b). An oval with double lines indicates the CC. In both figures, ovals with single lines, closed gray ovals, and closed black circles indicate the Mβ_LCLs, Mβ_SCSs, and meso-γ-scale convective cells associated with cumulonimbus clouds, respectively. The hatched regions show weak stratiform rainfall accompanied by cold pools.

6. Discussion

6.1 Multiscale structure

The multiscale structure of precipitation systems within the CC, when the Mβ_LCL was observed in the mature stage, is summarized in Fig. 21a. The CC consisted of a heavy rainfall region characterized by the Mβ_LCL, and a weak stratiform rainfall region located on the lee side of the Mβ_LCL. The weak rainfall was formed by hydrometeors that flowed toward the lee side in the upper- and middle-levels troposphere. The Mβ_LCL consisted of several Mβ_SCSs. Many of the Mβ_SCSs had band-shape structures in the southwest-northeast orientations.

Each Mβ_SCS was generated and maintained with the back-building-type: new meso-γ-scale cumulonimbus clouds were generated on the southwestern side of the Mβ_SCSs. The generations of new cumulonimbus clouds might be induced by the convergence of the inflow in the

shallow layer, and the outflow from old cumulonimbus clouds within the Mβ_SCSs. Therefore, the new cumulonimbus clouds should be located on the southern or south-southwestern side of the Mβ_SCSs. On the other hand, old meso-γ-scale clouds within the Mβ_SCSs propagated toward the northeast or east-northeast by the environmental LLJ. Consequently, each Mβ_SCS with a southwest-northeast orientation moved to the east within the Mβ_LCL. These characteristics are similar to that of the multiscale structure found by Iwasaki and Takeda (1989). In their case study, the band-shaped radar echoes were generated with an interval of about 1 hour, and their orientation had a large normal component to the direction of their movements.

On the other hand, the Mβ_LCL had an almost zonal orientation along the Baiu front. A slight difference of the axis directions between the Mβ_LCL and Mβ_SCSs is important in the multiscale structure in the present case. The orientation of the Mβ_LCL is considered to be controlled by Baiu frontal environmental factors. A small CIN around the CC is needed for convections within the CC to be generated. For the environmental warm and moist air inflow in the shallow layer, the lower temperature in the lower atmosphere above the shallow layer, produces the lower LFC and the smaller CIN. The decrease of CIN for the warm and moist air inflow was mainly induced by a vertical difference of the θ_e advection in the shallow layer, and the θ_e^* advection in the lower atmosphere above the shallow layer. The temperature and θ_e^* gradients in the lower atmosphere was mostly maintained for a long time as a characteristic feature of the Baiu frontal zone. Thus, a quasi-stationary meridional temperature gradient in the lower atmosphere effectively produces the small CIN for the warm and moist air inflow in the shallow layer. The zone of the large meridional temperature gradient extended almost zonally around the CC, and was consistent with the structure of the Mβ_LCL with the zonal orientation. It was not clearly determined in the present analysis how the temperature gradient became stationary and was maintained, but the reason is likely to be associated with the slow-moving depression and the Baiu front. Figure 6 shows not only the warm air southwesterly inflows on the southern side of the CC, but also the cold air westerly inflows on the northwestern side of the CC. These two flows, associated with the cyclonic circulation of the depression, seem to intensify the temperature gradient along the Baiu front. The maintenances of the high-θ_e southerly inflow in the shallow layer, and temperature gradient, are considered to be important environmental factors for the maintenance of the Mβ_LCL. Other effects of the convective organization might be important to control the orientation of the Mβ_LCL, but no evidences of the organizational mechanisms were found in the present analysis.

6.2 Life cycle of the Mβ_LCL

The Mβ_LCLs were periodically generated, with an interval of 5–6 hours in almost the same region, and showed a similar evolution in structure and process. The periodicity had some similarities to the characteristics of the multiscale structure described by Ninomiya et al. (1988a and 1988b). In their case, line-shaped mesoscale convective systems developed with a parallel orientation to the Baiu front over the Kyushu District and were generated with an interval of about 5 hours.

In the present case, the generation of the Mβ_LCLs (stage 1) was largely associated with the environmental forcing described in Section 6.1. On the other hand, it is inferred that the periodic evolution was largely due to the behavior of cold pools, generated by the Mβ_LCLs. The evolutions of the Mβ_LCLs, and variation of the multiscale structure are discussed by focusing on stages 2, 3, and 4 (Fig. 21b).

a. Stage 2: Development of the Mβ_LCL

The development of the Mβ_LCL was accompanied by the generation of a cold pool, and a weak rainfall region on the northern side of the Mβ_LCL. The cold pool was formed by the evaporation of a large amount of hydrometeors. The hydrometeors were produced by the convection in the Mβ_LCL, and were carried to evaporate toward the northern side. When Mβ_LCL-2 was present, the mean velocity around the Mβ_LCL-2 estimated by the Doppler radar had a large southerly component below 5 km in height (Fig. 20a) and was larger than that of the environmental wind at around 5 km in height (Fig. 20b). A large amount of hydrometeors was carried to the northern side of Mβ_LCL-2 by the large southerly component.

On the other hand, the southerly component had a local maximum at around 500 m in height on the southern side of the Mβ_LCLs (Fig. 4c). The large southerly component at around 5 km in height was considered to be the result of the convective vertical transport of the southerly momentum in the shallow layer on the southern side of the CC. However, it was difficult for the hydrometeors to evaporate in the Baiu frontal moist zone, which was present mainly on the northern side of the CC (Figs. 3c and 3d). It is inferred that the southwesterly dry inflow at around 700 hPa plays a role in the evaporation of the hydrometeors, because the θe on the southern side (windward side) of the CC at 700 hPa (Fig. 3d) and that above 1 km in height at RS2 (Fig. 4a) were significantly low.

Another characteristic feature in stage 2 is the time variation in height of the Mβ_SCSs (from Mβ_SCS-B to AMβ_SCS-2 in Fig. 17). The time variation is roughly explained by the rising of level of neutral buoyancy (LNB) due to the warm air advection. Additionally, it is inferred that the development of the cold pool also played a helpful role in the time variation in height. The small meridional component of the wind below 2 km in height at 1030–1200 JST in Fig. 20a was due to the small meridional component of the wind on the northern part of Mβ_SCS-D (Fig. 18d). It intensified the low-level convergence of the Mβ_SCSs, and the strong convergence supported the development of Mβ_SCS-D and AMβ_SCS-2. Here, the small meridional component of the wind on the northern part of Mβ_SCSs seems to be the expansion of the cold pool.

b. Stage 3: Decaying of the Mβ_LCL

The decaying of the Mβ_LCLs was accompanied by the expansion of the cold pools toward the south. The high-θe air inflow in the shallow layer was interrupted by the expansion of the cold pool. Then, the Mβ_LCLs decayed without significant propagation toward the south with the expansions of the cold pools. The location of the Mβ_LCLs is considered to be controlled by the quasi-stationary large-scale temperature gradient zone in the lower atmosphere rather than the θe gradient in the shallow layer.

In general, the expansion of the cold pool is classified into the gravity current. However, the temperature and pressure difference, estimated at about 2 K (Figs. 12a and 15) and about 1.5 hPa (Fig. 15), respectively, and the expansion speed, estimated at 6 m s^{-1}, were smaller than those of the gravity currents commonly known. A significant cold pool was also observed in the case studies reported by Ishihara et al. (1995) and Kawashima et al. (1995). The temperature and pressure contrasts were also estimated to be small in their cases. The comparatively small contrast and slow expansion might be associated with the slow generation of a cold pool, and might also be characteristic features of the cold pool under the moist environment in the Baiu frontal zone.

When the Mβ_LCLs were decaying, only the AMβ_SCSs were left as the sole strong rainfall elements making up the Mβ_LCL, and the weak rainfall region spread widely on the northwestern side of the AMβ_SCSs (Fig. 14). The characteristic features of the AMβ_SCSs show similarities to those of squall lines in terms of their fast movement, cold pool on the rear side, rear inflow, tilting structure, and deep convections as well as to those of the arc-shaped (bow-shaped) mesoscale convective systems reported by Weisman (1993) and Skamarock (1994). The modification from one of the Mβ_SCSs into the AMβ_SCS was not clearly detected by the Doppler radar because of the short ranges of the radars.

c. Stage 4 and 1: Wide spreading of the weak rainfall region and regeneration of the Mβ_LCL

When the cold pool expanded and the weak rainfall region spread widely, the low-level atmosphere became statically stable around the region in which Mβ_LCL-1 was previously located (Fig. 16a). The situation was maintained for about 3 hours, until Mβ_LCL-2 was generated. Mβ_LCL-2 was generated on the western side (windward side) of the CC. It is inferred that Mβ_LCL-2 was generated when the cold pool weakened and the environment for the generation of the Mβ_LCL was restored because the averaged velocities show that the southwesterly wind below 2 km in height associated with the environment was restored with the warm surface temperature on the northern side of Mβ_LCL-2 at around 10 JST in stage 1 (Figs. 12a and 20). Other mechanisms, such as

gravity waves, might be at work for the regeneration of Mβ_LCL-2, but no evidence became apparent in this analysis.

7. Summary

A meso-α-scale CC was observed in the Baiu frontal zone over the East China Sea, to the southwest of the Kyushu District, Japan on July 7, 1996. The CC had a long life span (about 20 hours) and a characteristic of stationariness. Consequently, the maximum rainfall for 12 hours was about 200 mm in a narrow area.

The CC was accompanied by a slow-moving, shallow depression on the northwestern side of the CC. The cyclonic circulation of the depression brought a significantly warm and moist inflow toward the CC in the shallow layer. The LFC decreased by the inflow toward the zone in which the meridional temperature gradient in the lower atmosphere was large, and the CC developed. These conditions were maintained for a long time because of the slow movement of the depression.

The evolution of the CC was divided into three stages: developing, mature, and decaying stages. In the mature stage, a multiscale structure of the CC, summarized in Fig. 21a, was observed. The CC consisted of a convective rainfall region, which was characterized by the Mβ_LCL, and a weak rainfall region on the lee side of the Mβ_LCL. The Mβ_LCLs extended zonally along the large temperature gradient zone in the lower atmosphere. They were generated twice with an interval of 5–6 hours in the mature stage, and the life span was about 2.5 hours. Two or more Mβ_LCLs were not simultaneously present in the CC. The Mβ_LCL consisted of several Mβ_SCSs. Each Mβ_SCS had a periodic interval of about 1 hour and a life span of 1–3 hours. Many of them were organized into band shapes with a southwest to northeast orientation in association with the environmental southwesterly wind in the lower atmosphere. Moreover, the Mβ_SCS consisted of several meso-γ-scale cumulonimbus clouds. The Mβ_SCSs were maintained by successive generations of new cumulonimbus clouds on the southwestern side of each Mβ_SCS (backbuilding type).

The evolution of the Mβ_LCL, which is summarized in Fig. 21b, is divided into four stages as follows.

Stage 1: Generation of the Mβ_LCL.

Stage 2: Development of the Mβ_LCL and generations of the weak rainfall region and the cold pool on the northern side of the Mβ_LCL.

Stage 3: Decaying of the Mβ_LCL and expansion of the cold pool accompanied with the development of the AMβ_SCS.

Stage 4: Widely spreading of the weak rainfall region.

The development of the Mβ_LCL was accompanied by the generation of a cold pool on the northern side of the Mβ_LCL. The cold pool significantly developed and intensified the convergence of the Mβ_SCS in the Mβ_LCL. One of the Mβ_SCSs was modified into the AMβ_SCS in association with the intensification of the cold pool about 2 hours after the generation of the Mβ_LCL. The AMβ_SCS had characteristics similar to those of squall lines: a tilting deep convection, fast-moving, and the low-level inflow on the rear side. The development of the AMβ_SCS was accompanied by the decaying of the Mβ_LCL. The decaying was associated with the expansion of the cold pool. After the expansion of the cold pool, only the weak rainfall region spread widely for about 3 hours, because of the stable condition in the expanded cold pool. Another Mβ_LCL was generated on the western side of the CC by the restoration of the favorable environment for the generation of the Mβ_LCL after the cold pool weakened.

Acknowledgements

In the present study, we used TREX data collected by the JMA, the MRI, the Ocean Research Institute (ORI) of the University of Tokyo, the Institute of Space and Astronautical Science (ISAS) of the University of Tokyo,[1] the Communications Research Laboratory (CRL),[2] and the HyARC of Nagoya University. We thank Dr. Kazuo Saito (MRI), Prof. Hiroshi Niino (ORI), and Mr. Yoshinobu Tanaka (JMA) for providing these data. Special thanks are due to Dr. Hiromu Seko (MRI) and Prof. Hiroshi Uyeda (HyARC) for their beneficial com-

1 Present Organization: Japan Aerospace Exploration Agency (JAXA).

2 Present Organization: National Institute of Information and Communications Technology (NICT).

ments and participation in discussions. Thanks are extended to the editor and two anonymous referees of this paper for their useful comments.

References

Akiyama, T., 1978: Mesoscale pulsation of convective rain in medium-scale disturbances developed in Baiu front. *J. Meteor. Soc. Japan*, **56**, 267–283.

Bluestein, H.B. and M.H. Jain, 1985: Formation of mesoscale lines of precipitation—Severe squall lines in Oklahoma during the spring. *J. Atmos. Sci.*, **42**, 1711–1732.

Ishihara, M., Y. Fujiyoshi, A. Tabata, H. Sakakibara, K. Akaeda, and H. Okamura, 1995: Dual Doppler radar analysis of an intense mesoscale rainband generated along the Baiu front in 1988: Its kinematical structure and maintenance process. *J. Meteor. Soc. Japan*, **73**, 139–163.

Iwasaki, H. and T. Takeda, 1989: Behavior of cumulonimbus-cloud groups in a slow-moving mesoscale cloud cluster over the ocean. *J. Meteor. Soc. Japan*, **67**, 575–586.

Kato, T., 1998: Numerical simulation of the band-shaped torrential rain observed over southern Kyushu, Japan on 1 August 1993. *J. Meteor. Soc. Japan*, **76**, 97–128.

———, K. Kurihara, H. Seko, and H. Goda, 1998: Verification of the MRI-Nonhydrostatic-Model Predicted Rainfall during the 1996 Baiu Season. *J. Meteor. Soc. Japan*, **76**, 719–735.

Kawashima, M., K. Tsuboki, and T. Asai, 1995: Maintenance mechanism and thermodynamic structure of a Baiu frontal rainband retrieved from dual Doppler radar observations. *J. Meteor. Soc. Japan*, **73**, 717–735.

Leary, C.A. and R.A. Jr. Houze, 1979: The structure and evolution of convection in tropical cloud cluster. *J. Atmos. Sci.*, **36**, 437–457.

Maddox, R.A., 1980: Mesoscale convective complexes. *Bull. Amer. Meteor. Soc.*, **61**, 1374–1387.

Matsumoto, S. and T. Akiyama, 1969: Some characteristic features of the heavy rainfalls observed the western Japan on July 9, 1967 Part 1: Mesoscale structure and short period pulsation. *J. Meteor. Soc. Japan*, **47**, 255–266.

——— and Y. Tsuneoka, 1969: Some characteristic features of the heavy rainfalls observed the western Japan on July 9, 1967 Part 2: Displacement and life cycle of mesoscale rainfall cells. *J. Meteor. Soc. Japan*, **47**, 267–278.

Ninomiya, K., 1983: Internal-gravity-wave-like variations of temperature, humidity and wind observed in the troposphere downstream of rainfall area. *J. Meteor. Soc. Japan*, **61**, 163–169.

Ninomiya, K., T. Akiyama, and M. Ikawa, 1988a: Evolution and fine structure of a long-lived meso-α-scale convective system in a Baiu frontal zone. Part I: Evolution and meso-β-scale characteristics. *J. Meteor. Soc. Japan*, **66**, 331–350.

———, ———, and ———, 1988b: Evolution and fine structure of a long-lived meso-α-scale convective system in a Baiu frontal zone. Part II: Meso-γ-scale characteristics of precipitation. *J. Meteor. Soc. Japan*, **66**, 351–371.

Orlanski, I., 1975: A rational subdivision of scales for atmospheric processes. *Bull. Amer. Meteor. Soc.*, **56**, 527–530.

Seko, H., 2000: Study of the shapes and maintenance mechanisms of meso-β scale line-shaped precipitation systems in the middle-latitudes. (Doctoral dissertation) (in Japanese).

Skamarock, W.C., M.L. Weisman, and J.B. Klemp, 1994: Three-dimensional evolution of simulated long-lived squall lines. *J. Atmos. Sci.*, **51**, 2563–2584.

Weisman, M.L., 1993: The genesis of severe, long-lived bow echoes. *J. Atmos. Sci.*, **50**, 644–670.